Mon. Not. R. Astron. Soc. **335,** 698–706 (2002)

The asteroseismological potential of the pulsating DB white dwarf stars CBS 114 and PG 1456+103

G. Handler,[1]★ T. S. Metcalfe[2] and M. A. Wood[3]

[1]*South African Astronomical Observatory, PO Box 9, Observatory 7935, South Africa*
[2]*Theoretical Astrophysics Centre, Institute of Physics and Astronomy, Aarhus University, DK-8000 Aarhus C, Denmark*
[3]*Department of Physics and Space Sciences & SARA Observatory, Florida Institute of Technology, Melbourne, FL 32901, USA*

Accepted 2002 May 2. Received 2002 May 2; in original form 2002 April 12

ABSTRACT

We have acquired 65 h of single-site time-resolved CCD photometry of the pulsating DB white dwarf star (DBV) CBS 114 and 62 h of two-site high-speed CCD photometry of another DBV, PG 1456+103. The pulsation spectrum of PG 1456+103 is complicated and variable on time-scales of approximately 1 week and could only partly be deciphered with our measurements. The modes of CBS 114 are more stable in time and we were able to arrive at a frequency solution somewhat affected by aliasing, but still satisfactory, involving seven independent modes and two combination frequencies. These frequencies also explain the discovery data of the star, taken 13 yr earlier.

We find a mean period spacing of 37.1 ± 0.7 s significant at the 98 per cent level between the independent modes of CBS 114 and argue that they are caused by non-radial g-mode pulsations of spherical degree $\ell = 1$. We performed a global search for asteroseismological models of CBS 114 using a genetic algorithm, and we examined the susceptibility of the results to the uncertainties of the observational frequency determinations and mode identifications (we could not provide m values). The families of possible solutions are identified correctly even without knowledge of m. Our best-fitting model suggests $T_{\rm eff} = 21\,000$ K, $M_* = 0.730$ M$_\odot$ and $\log(M_{\rm He}/M_*) = -6.66$, $X_{\rm O} = 0.61$. The latter value of the central oxygen mass fraction implies a rate for the $^{12}{\rm C}(\alpha, \gamma)^{16}{\rm O}$ nuclear reaction near $S_{300} = 180$ keV b, consistent with laboratory measurements.

Key words: stars: individual: CBS 114 – stars: individual: PG 1456+103 – stars: oscillations – stars: variables: other.

1 INTRODUCTION

The helium-atmosphere DB white dwarf stars are very interesting from the standpoint of stellar structure and evolution. The chemical evolution of their atmospheres cannot be satisfactorily explained to date (see Shipman 1997 for a review). In particular, the presence of the so-called DB gap, the absence of DB white dwarfs between temperatures of ~30 000–45 000 K (Liebert 1986), is poorly understood. It is also not clear whether DBs are mostly produced by single-star evolution or whether a significant fraction of them originates from binary progenitors.

The examination of these problems can be aided by asteroseismology – the study of the interiors of pulsating stars via the analysis of their normal-mode spectra. Fortunately, a class of pulsating DB white dwarf stars (hereinafter DBVs) exists, and their prototype, GD 358, is one of the classical examples for the successful application of asteroseismological methods (Winget et al. 1994; Vuille et al. 2000).

Compared with other classes of pulsating star, the DBVs seem quite promising candidates for asteroseismology: their mode spectra are shown or believed to be rich, and pulsation theory for these stars is quite advanced and well tested. For instance, the central oxygen abundance of the models has been shown to have a measurable effect on the pulsation frequencies (Metcalfe, Winget & Charbonneau 2001), and the possible presence of a ^{3}He/^{4}He transition zone caused by chemical diffusion has also been shown to produce a measurable effect (Montgomery, Metcalfe & Winget 2001), although recent observations have ruled out this possibility (Wolff et al. 2002). In addition, the recently developed application of genetic-algorithm-based model fitting to DBV mode spectra (Metcalfe, Nather & Winget 2000) allows an objective and effective exploration of parameter space to find an optimal model for the observations.

The application of these methods to DBVs other than GD 358 is, however, hampered by a lack of suitable observational data. Most of these stars are rather faint (around 16th magnitude), which requires

★ E-mail: handler@astro.univie.ac.at

the use of 2-m class telescopes to acquire suitable data with photomultiplier detectors. However, time on these telescopes is generally oversubscribed and long runs are difficult to obtain. With the advent of CCD detectors and with the development of systems capable of acquiring measurements of high time resolution, the DBVs are now in reach of smaller telescopes. We have therefore started to acquire measurements aiming to make as many DBVs as possible accessible to asteroseismology.

The pulsations of the DB white dwarf star CBS 114 were discovered by Winget & Claver (1988, 1989), who reported multiperiodic oscillations with peak-to-peak light variations up to 0.3 mag and with a time-scale of approximately 650 s. PG 1456+103 (hereinafter referred to as PG 1456) was reported as a DBV by Grauer et al. (1988). These authors reported multiperiodic pulsations with dominant periodicities of between 420 and 850 s and maximum peak-to-peak amplitudes around 0.15 mag. As no further observations of either of these stars have been published, we deemed it worthwhile to obtain larger data sets to study the pulsations of CBS 114 and PG 1456 in more detail.

2 OBSERVATIONS

Most of our measurements were acquired as differential CCD photometry with the 0.75-m telescope at the Sutherland station of the South African Astronomical Observatory (SAAO), at which we had been allocated 3 weeks of observing time.

We used the University of Cape Town CCD camera (O'Donoghue 1995). Its CCD was operated in full-frame mode to acquire a maximum number of local comparison stars. We used 2×2 or 3×3 pre-binning depending on seeing, which results in readout times of approximately 2–3 s. For the faint CBS 114 ($B \approx 17.2$ as estimated from our CCD frames compared with PG 1456+103), we used integration times of 27 or 28 s to obtain one frame per 30 s, and we used 20-s integrations for PG 1456. No filter was used to maximize the number of photons detected. In every clear night, sky flat-fields were taken during twilight.

In addition, we acquired measurements of PG 1456 with the 0.9-m SARA telescope at Kitt Peak National Observatory (Arizona), to reduce the aliasing problem in the frequency analysis. The CCD used is an Apogee AP7p, with a back-illuminated SITe SIA-502AB 512×512 detector. The pixels are 24 μm square, or 0.75 arcsec pixel^{-1}. Read noise for the camera is 12.2 electrons rms, and the gain is 6.1 electrons ADU^{-1}. We used integration times of typically 30 s, and our readout time was approximately 7 s. Again, we took sky flats during each twilight. Our measurements are summarized in Table 1.

We started data reduction with the corrections for bias, dark counts (SARA measurements only) and flat-field. Mean weekly flat-fields were used for the SAAO data sets and combined nightly flats for the SARA frames. Photometric measurements on these reduced frames were made with the program MOMF (Kjeldsen & Frandsen 1992), which applies a combination of point spread function (PSF) and aperture photometry relative to a user-specified ensemble of comparison stars. No variability of any star other than the targets in the different CCD fields was found, and the comparison star ensemble resulting in the lowest scatter in the target-star light-curves was chosen.

The resulting differential light curves were corrected for differential colour extinction and for correlations with seeing. For CBS 114, it was sometimes also found necessary to de-trend the data with (x, y) position of the star on the chip because of flat-field errors. Residual low-frequency trends in the data (not found to be coherent over the time-span of the observations, hence judged not to be intrinsic to the stars) were removed by means of low-order polynomials.

Table 1. Journal of the observations. The SARA measurements were obtained between JD 245 1987 and 2451990; the remainder are SAAO data. *N* is the number of frames taken.

CBS 114			PG 1456+103		
Run start JD 245 0000	Length (h)	*N*	Run start JD 245 0000	Length (h)	*N*
1940.421	3.32	403	1940.570	1.44	225
1941.400	3.74	450	1941.609	0.55	87
1942.394	4.00	446	1942.570	1.49	219
1943.446	1.30	143			
1944.427	3.40	404	1944.573	1.51	233
1945.397	4.25	484	1945.577	1.44	209
1946.386	4.17	435	1946.567	1.75	267
1954.379	0.68	80			
1955.359	4.20	382	1955.539	2.50	410
1956.357	4.30	513	1956.539	2.62	400
1957.353	4.25	495	1957.533	2.74	442
1959.346	4.38	464	1959.530	2.93	449
1960.346	4.30	511	1960.530	0.55	81
			1987.929	2.71	251
			1988.898	3.34	277
			1989.882	3.60	349
1996.249	4.17	497	1996.426	5.83	897
1997.239	4.32	511	1997.423	5.88	909
1998.235	4.36	520	1998.422	4.37	617
1999.355	1.37	156	1999.416	4.99	692
2001.319	1.38	107	2001.415	4.42	681
2002.252	2.77	324	2002.373	6.94	808
Total	64.66	7325		61.60	8503

Finally, the times of measurement were transformed to a homogeneous time base. We chose terrestrial time (TT) as our reference for measurements on the surface of the Earth and applied a correction to account for the motion of the Earth around the barycentre of the Solar system. As this barycentric correction varied up to ±1 s throughout a run, we applied it point by point. Our final time base therefore is barycentric Julian ephemeris date (BJED). The reduced time series were subjected to frequency analyses; we show example light curves in Figs 1 and 2. The typical rms scatter per single data point is around 40–50 mmag for CBS 114, and for PG 1456 approximately 15 mmag (SAAO data) and 11 mmag (SARA data).

3 FREQUENCY ANALYSIS

Our frequency analysis was performed with the program PERIOD98 (Sperl 1998). This package applies single-frequency power spectrum analysis and simultaneous multifrequency sine-wave fitting, but also has some advanced options. In particular, it can be used to calculate optimal solutions for multiperiodic signals including harmonic, combination and equally spaced frequencies, which are often found in the analysis of the light curves of pulsating white dwarf stars.

3.1 CBS 114

A frequency analysis of single-site data of a multiperiodic variable in the presence of noise is difficult because of aliasing; extreme caution is required. However, the structure and extent of our data set aids us in this effort.

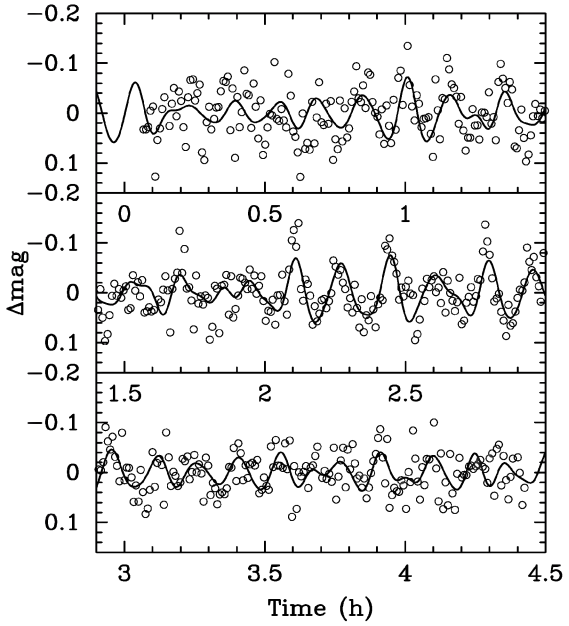

Figure 1. An example light curve of CBS 114; a multifrequency fit is included as well. Although the data are not of impressive quality caused by the faintness of the star, the multiperiodic pulsations are clearly visible.

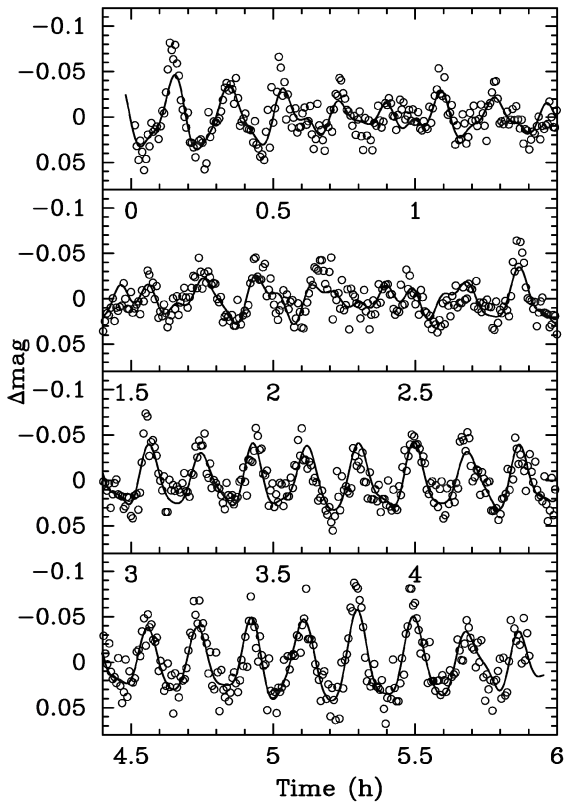

Figure 2. An example light curve of PG 1456+103 with a multifrequency fit. As the star is 1.3 mag brighter than CBS 114, the data are of much better quality; the multiperiodic pulsations are readily visible as well.

We started by calculating nightly amplitude spectra of our data. The amplitude spectra of the individual nights were quite similar, with a number of dominant peaks always occurring at similar frequencies. However, some variations in the individual amplitudes were noted.

As the next step, we combined the three 1-week data sets (which are very similar in length and extent) and we computed their amplitude spectra and that of all 3 weeks combined. They are shown in Fig. 3, which shows six dominant structures between 1.4 and 2.6 mHz and some further signals that could be combination frequencies.

Some trial pre-whitening within the strongest features convinced us that all of them are dominated by one signal each. Consequently, we determined their frequencies by examining the combined, the weekly and the average of the weekly amplitude spectra and by least-squares fitting to the light curves. In this way, we could rule out a number of alias frequencies because they gave unreasonable results if adopted. However, in some cases, no unambiguous decision could be made.

Having determined the best set of frequencies, we refined their values by calculating an optimal solution for the whole data set, pre-whitened it from the data and calculated the amplitude spectrum of the residuals (upper panel of Fig. 4). Because of the temporal changes in the weekly amplitude spectra, it is not surprising that some residual mounds of amplitude remained near the dominant frequencies.

We examined the frequencies of these features and their aliases and performed trial pre-whitening to check for any multiplet structure possibly present. No such evidence was found. We then fitted our best frequencies to the individual nights longer than 3 h

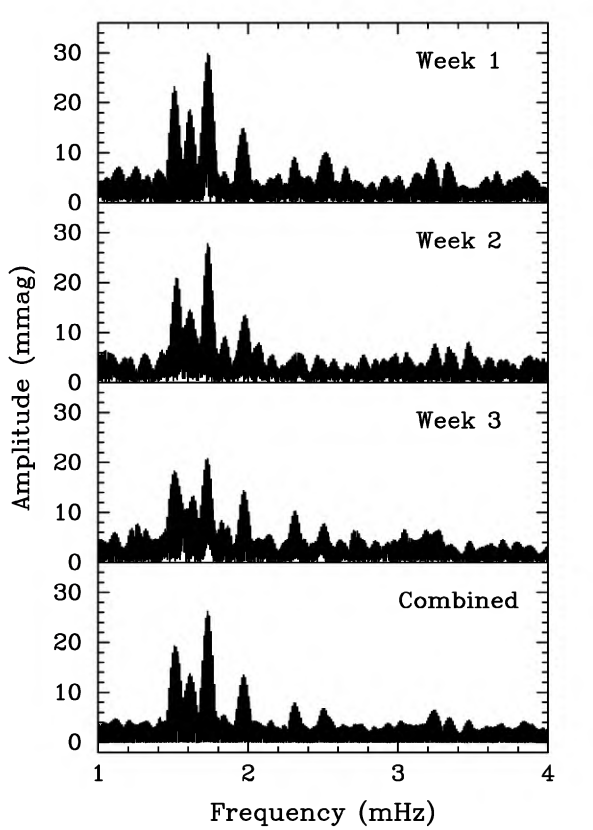

Figure 3. Weekly and combined amplitude spectra of our CBS 114 data. The same peaks are always present, but with somewhat variable amplitudes.

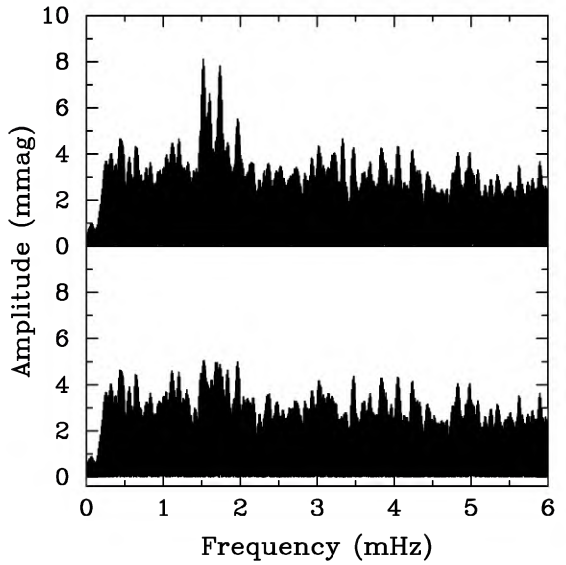

Figure 4. Upper panel, residual amplitude spectrum after pre-whitening the best multifrequency solution for our measurements of CBS 114, assuming constant amplitudes and phases over the whole data set. Lower panel, residual amplitude spectrum after pre-whitening the same frequency solution, but allowing for amplitudes and phases to vary over half-week intervals.

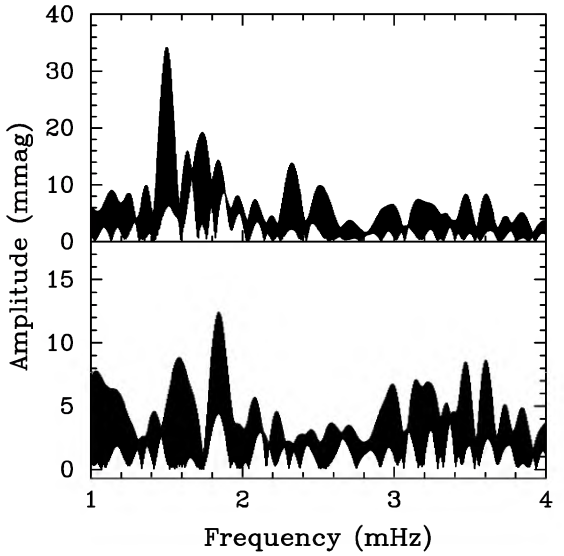

Figure 5. Upper panel, amplitude spectrum of the measurements by Winget & Claver (1988, 1989). Lower panel, residual amplitude spectrum after pre-whitening the first six frequencies determined from our observations.

(ensuring that the dominant structures are resolved) and determined their amplitudes, phases and corresponding error estimates (following Montgomery & O'Donoghue 1999). We found that significant amplitude and phase changes occurred over time-scales of 3–4 d, and that either amplitude or phase variability alone is not sufficient to explain the observations – both are present.

As we cannot determine the cause of these variations, we treated them phenomenologically and calculated our final multifrequency solution with constant frequencies as determined previously, but with amplitudes and phases variable over half-week periods. In this way, we can determine ranges of the amplitudes of the dominant signals, and most of the residual mounds in the amplitude spectrum are thus removed (lower panel of Fig. 4). In Table 2, we list the best multifrequency solution determined with this method.

Table 2. Multifrequency solution for CBS 114. For frequencies labelled with a minus sign, the negative daily alias ($f_i - 11.60\mu$Hz) may be the correct frequency, and for frequencies labelled with a plus sign, the positive daily alias ($f_i + 11.60\mu$Hz) cannot be ruled out as the correct value. Amplitudes are listed in the ranges they assumed during the observations.

ID	Freq. (μHz)	Period (s)	Amp. (2001) (mmag)	Amp. (1988) (mmag)
f_1	1518.75^-	658.43	16–33	33
f_2	1613.12	619.91	10–17	15
f_3	1729.73	578.13	22–37	18
f_4	1969.60	507.71	11–17	<5
f_5	2306.38^+	433.58	4–12	13
f_6	2509.89^-	398.42	4–10	9
$f_1 + f_3$	3248.48	–	5–7	<7
$f_2 + f_3$	3342.85	–	2–8	<6
f_7	1835.64^{+-}	544.77	<4.2	13

3.1.1 *Re-analysis of Winget & Claver's data*

Although the measurements by Winget & Claver (1988, 1989) only comprise 5.2 h of data obtained over two nights, we can still use them for a comparison with our results. The amplitude spectrum of these measurements (upper panel of Fig. 5) shows dominant features at frequencies agreeing very well with those determined from our data. Consequently, we fitted the first six frequencies from Table 2 to these measurements and noticed that they were consistent with the older data. We therefore determined corresponding frequencies, amplitudes and phases, subtracted this fit from the data and calculated a residual amplitude spectrum, which is shown in the lower panel of Fig. 5, revealing the presence of yet another signal.

A variation at this frequency is also present in our new observations, although its amplitude is below our detection threshold. Consequently, we include it in our final frequency solution for the combined data sets (Table 2). We note some more suspected signals in the lower panel of Fig. 5, but owing to the small amount of data we do not push the analysis further. We have therefore detected altogether seven independent pulsation frequencies and two combination signals in the available light curves of CBS 114.

3.2 PG 1456

Owing to our two-site coverage of the light variations of PG 1456, the frequency analysis should be comparatively easy. However, initial trials showed that the pulsational amplitudes and frequencies of this star are also somewhat variable, and as our light curves from the first 2 weeks are rather short, they complicate the analysis if the total data set is used. Consequently, we used the JD 245 1987–JD 245 2002 two-site measurements as our primary data set for the frequency analysis; the remaining data were used for comparison purposes and consistency checks. Fig. 6 shows some pre-whitening steps in these two main subsets of data.

A signal (f_B) not present in the early SAAO observations reached considerable amplitude in the combined two-site data obtained

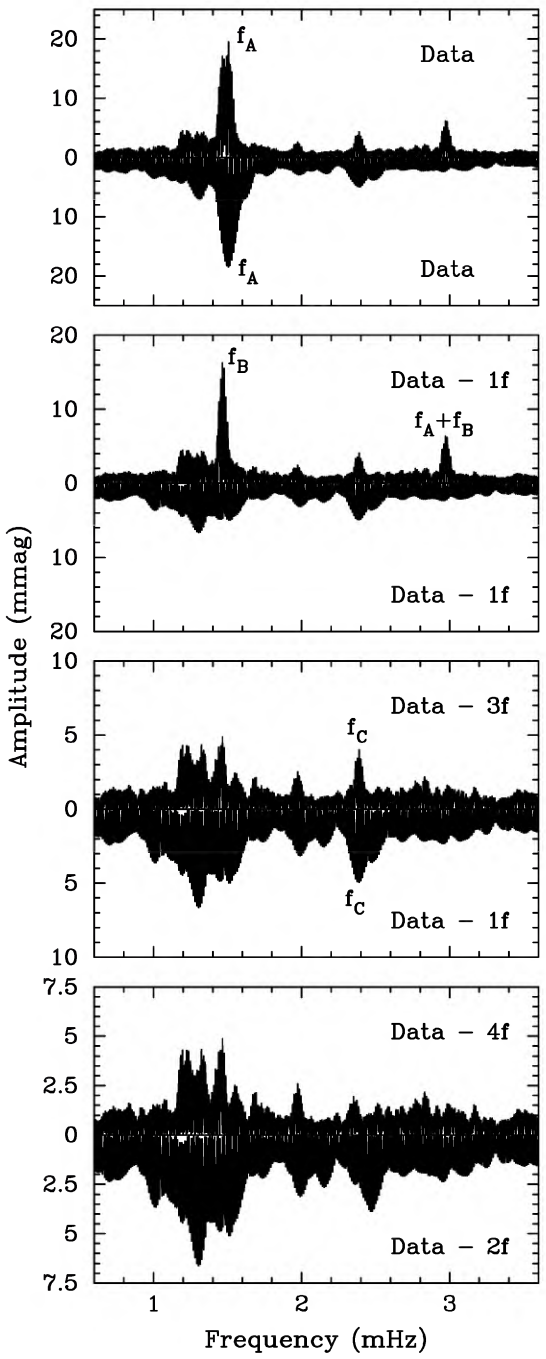

Figure 6. Amplitude spectra of our measurements of PG 1456. The upper halves of the panels are for the two-site JD 245 1987–JD 245 2002 data, whereas the lower, mirrored, halves originate from the preceding single-site observations. Uppermost panel, original data. Second panel, data after pre-whitening of the dominant frequency. Another frequency and a combination are detected only in the two-site data. Third panel, another mode is found in all the data. Lowest panel, the residual amplitude spectra; more signals are clearly present.

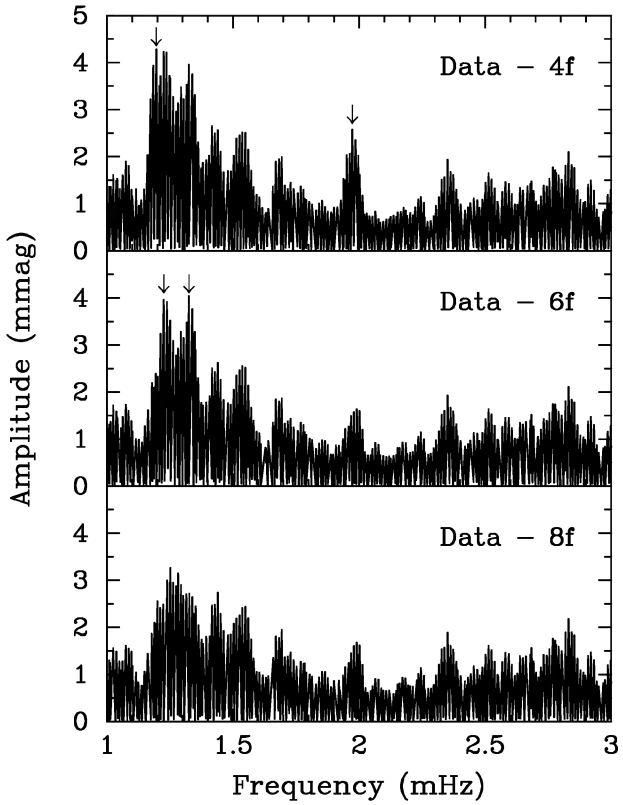

Figure 7. Pre-whitened amplitude spectra of our measurements of PG 1456. The arrows in the individual panels indicate further possible signals that are pre-whitened in the following panels.

approximately 7 weeks later; we note that this is not caused by an aliasing problem. As a matter of fact, the amplitude of this signal was still increasing during the latter measurements. It had approximately 12 mmag in the SARA data, but 18 mmag in the last set of SAAO measurements, in which it also showed a significant phase variation. A combination frequency ($f_A + f_B$) not present initially also appeared in the two-site data. On the other hand, the signal f_C was found to be constant in amplitude and phase over the whole data set, and f_A was constant in amplitude but showed a slight frequency shift of approximately 0.4 μHz between our two subsets of data.

The residual amplitude spectra in the lowest panel of Fig. 6 still show a number of interesting peaks, several of which may be real. To estimate the richness of the frequency spectrum of PG 1456, we performed further pre-whitening in the two-site data (still checking with the early SAAO measurements), taking the temporal variations of f_B into account. The resulting amplitude spectra are shown in Fig. 7.

It becomes clear that the light variations of PG 1456 are quite complicated and that our data set is not sufficient for finding all the frequencies present. A preliminary multifrequency solution is given in Table 3.

A few comments are still necessary. Signals in the region around 1970 μHz are present in both data sets with similar amplitude (e.g. the 1973.4 μHz signal in Table 3), but their frequencies are different by 5 μHz, even taking aliasing into account. The dominant frequency region in the residual single site-data is around 1304 μHz, but neither this frequency nor its aliases are present in the two-site data. It seems that only intensive multisite observations will make a good understanding of the frequency spectrum of PG 1456 possible.

The periods we determined are in very good agreement with those detected by Grauer et al. (1988). Regrettably, a detailed comparison

Table 3. Preliminary multifrequency solution for PG 1456. Whereas we are sure about the frequencies f_A to f_C, the other values may be affected by aliasing. Amplitudes are given for both the two-site measurements (left-hand column) and the preceding single-site SAAO data. Because of amplitude and frequency variability, error estimates are only given for amplitudes of apparently constant signals.

ID	Freq. (μHz)	Period (s)	Amp. (mmag)	Amp. (mmag)
		Certain detections		
f_A	1505.9	664.1	18.9 ± 0.3	18.5 ± 0.6
f_B	1465.4	682.4	$11.7 - 18.4$	–
$f_A + f_B$	2971.3	–	$5.7 - 6.8$	–
f_C	2387.9	418.8	4.0 ± 0.3	5.0 ± 0.6
		Possible further signals		
	1195.9	836.2	4.4 ± 0.3	4.4 ± 0.6
	1973.4	506.7	2.7 ± 0.3	–
	1224.8	816.5	3.9 ± 0.3	–
	1324.9	754.8	3.9 ± 0.3	–

of these periods is impossible as the discovery data are no longer available (Grauer, private communication).

4 INTERPRETATION OF THE OBSERVATIONAL RESULTS

4.1 CBS 114

The independent pulsation periods of CBS 114 as listed in Table 2 seem to have similar spacing. We therefore searched for and determined their mean spacing by calculating the Fourier power spectrum of the period values with unit amplitude (Handler et al. 1997), which we show in Fig. 8. A mean period spacing (significant at the 98 per cent level) is indicated, amounting to 37.1 ± 0.7 s. This result is corroborated by a Kolmogorov–Smirnov test (not shown).

We interpret this preferred period separation as a sign of the excitation of a number of pulsational radial overtones with the same spherical degree ℓ. Some small deviations around its mean value (see Fig. 9 in Section 5) are an indication of mode trapping. The presence of a preferred period separation is predicted by asymptotic theory (Tassoul 1980), and was already observed within, for example, the $\ell = 1, m = 0$ modes of GD 358 (Winget et al. 1994; Vuille et al. 2000), for which a mean period spacing of 39.2 s was found. In addition, Bradley & Winget (1994) showed that the systematic deviations from this mean spacing were caused by mode trapping.

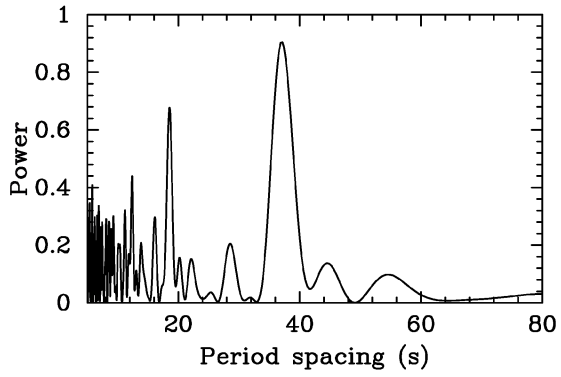

Figure 8. Search for a preferred period separation within the independent signals in the light curves of CBS 114. A spacing of 37.1 s and its harmonics dominate this diagram.

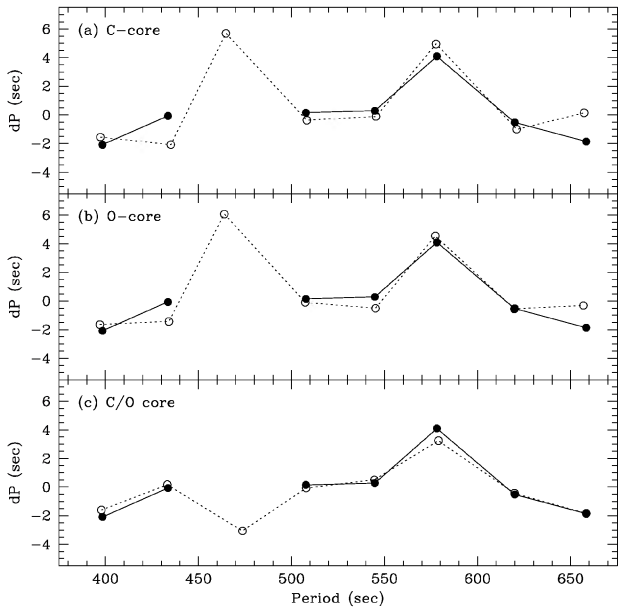

Figure 9. The observed periods of CBS 114 (solid) and the optimal model periods found by the genetic algorithm (open) plotted against the deviations from the mean period spacing, assuming a core of (a) pure C, (b) pure O and (c) mixed C/O (see the text for complete details).

We cannot directly identify the ℓ, m values of the modes we observed in CBS 114 because of the lack of any rotational m-mode splitting in our frequency spectra. However, it seems very likely that the independent modes of CBS 114 are all $\ell = 1$: if we saw a mixture of ℓ values, we would not expect to find such a significant mean period spacing. Therefore, the modes we observed must originate exclusively (or at least predominantly) from the same ℓ. They should be $\ell = 1$ or 2 as the effects of geometrical cancellation (Dziembowski 1977) are expected to render modes of higher ℓ photometrically undetectable.

The mean period spacing between consecutive overtones of a pulsating white dwarf star is a measure of its mass (Kawaler 1987). If the modes of CBS 114 were $\ell = 1$, their mean period spacing would be consistent with the star being a bit more massive than GD 358. However, if the modes were all $\ell = 2$, CBS 114 would need to have a mass below 0.3 $M_\odot$ (see Bradley, Winget & Wood 1993). Such a low mass is inconsistent with the spectroscopic gravity of the star (Beauchamp et al. 1999) and would be quite unusual in the light of the mass distribution of the DB white dwarf stars (Beauchamp et al. 1996).

Based on these arguments, we suggest that CBS 114 is a DBV star pulsating predominantly in non-radial g-modes of spherical degree $\ell = 1$. We note that its individual pulsation periods, especially that of longer period modes, are very similar to that of GD 358.

4.2 PG 1456

The interpretation of the frequency spectrum of PG 1456 is more difficult. A search for a mean period spacing such as in the previous

section did not give a significant result. This suggests that the modes we detected are not of the same ℓ or that the star is a fast rotator. The modes of $m \neq 0$ would then mask the possible patterns of equally spaced periods.

Approximately half of the independent periods we detected or suspect are similar to periods of GD 358, but the others are not. We are therefore unable to interpret the mode spectrum of PG 1456 at this stage. Extensive multisite observations, e.g. with the Whole Earth Telescope (Nather et al. 1990), are required to understand the pulsations of this star.

5 ASTEROSEISMOLOGY OF CBS 114

Using the optimization method developed by Metcalfe et al. (2000, 2001), we performed a global search for the optimal model parameters to fit the seven independent pulsation periods for CBS 114 listed in Table 2. The method uses a parallel genetic algorithm to minimize the root-mean-square (rms) differences between the observed and calculated periods for models with effective temperatures ($T_{\rm eff}$) between 20 000 and 30 000 K, total stellar masses (M_*) between 0.45 and 0.95 $M_\odot$, and helium layer masses with $-\log(M_{\rm He}/M_*)$ between 2.0 and ~7.0. This technique has been shown to find the globally optimal set of parameters consistently among the many possible combinations in the search space, but requires between ~10 and 4000 times fewer model evaluations than an exhaustive search of parameter space to accomplish this (depending on the number of free parameters), with a failure rate $<10^{-5}$.

We assumed that all of the observed modes had spherical degree $\ell = 1$ (as suggested in Section 4.1) and azimuthal order $m = 0$. The latter assumption can bias our determination of the *particular* set of model parameters that produces the optimal fit to the data, but if the rotation period is ~1 d, any set of periods drawn from $m = (-1, 0, +1)$ will produce essentially the same overall picture of the parameter space. We demonstrated this general behaviour by generating C-core fits to 100 data sets for GD 358 that used randomly selected m-components from those identified in Winget et al. (1994), and the $m = 0$ values for $k = 12, 18$ (for which no triplet structure was found). In every case, the optimal set of model parameters fell within the same families of good solutions that were identified using the $m = 0$ modes. Thus, when the spherical degree of the modes is known, the model-fitting procedure correctly identifies the *families* of possible solutions even when the values of m are unknown. Furthermore, we found that the optimal solutions fell into the various families within parameter space in proportion to the relative fitness of that family when only $m = 0$ modes were used for the fit. For example, if a family has a peak fitness in the $m = 0$ case that is 3σ better than any other family, then the use of $m \neq 0$ modes will identify an optimal solution in this same family with ~50 per cent probability. This means that if one of the families produces much better solutions than the others, we can be reasonably confident that we have at least identified the correct family of solutions.

5.1 Carbon-core fit

Assuming a pure C core extending to a fractional mass of $0.95m/M_*$, the optimal set of model parameters found by the genetic algorithm were

$T_{\rm eff} = 24\,600$ K

$M_* = 0.655\,M_\odot$

$\log(M_{\rm He}/M_*) = -3.96,$

with rms period residuals $\sigma_P = 1.02$ s. The observed and calculated periods are shown in the top panel of Fig. 9 plotted against the deviations from the mean period spacing (dP), which were calculated using the same set of periods in both cases. Each point in this representation of the data is independent of the others, unlike a period spacing diagram using ΔP ($\equiv P_{k+1} - P_k$; cf. Bradley & Winget 1994). Note that the genetic algorithm only fits the periods of the pulsation modes, and the agreement between the deviations from the mean period spacing is simply a reflection of the overall quality of the match.

As noted in Table 2, the daily aliases of several of the identified modes in CBS 114 cannot be ruled out entirely. We can assess the impact of this uncertainty on the final set of optimal model parameters by repeating the fitting procedure using one or more of the alias periods. However, since the genetic algorithm fitting method with three free parameters is only approximately 10 times more efficient than calculating the entire grid of models, it is better to calculate the pulsation periods of all 10^6 models if we intend to repeat the procedure more than a few times. As there are four periods with a total of five possible aliases, we chose to calculate the entire grid of models. This allows us to check the answer that resulted from the genetic algorithm fit, and will enable us to generate C-core fits very quickly in the future for any additional data sets on DBV white dwarf stars.

All C-core models with rms period residuals smaller than 2.22 s are shown in the top half of Fig. 10, which includes front and side views of the entire search space. Each point in the left-hand panel corresponds to a point in the right-hand panel, and the darkness of a point indicates the relative quality of the match with the observations. Black points are within $\Delta\sigma_P = 0.03$ s of the optimal model, and the four progressively lighter shades of grey correspond to models within 3, 10, 25 and 40 times this difference. The

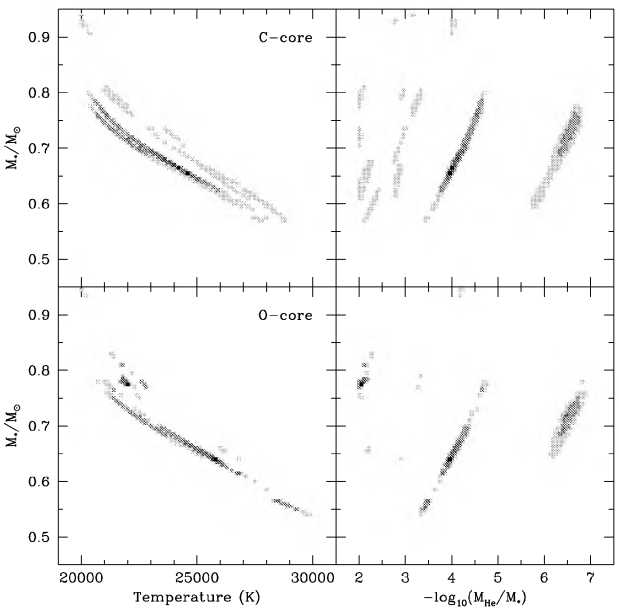

Figure 10. Front and side views of the search space assuming a C-core (top panels) and an O-core (bottom panels). Square points mark the location of models that yield a reasonable match to the periods observed for CBS 114. The darkness of a point indicates the relative quality of the match (see the text for complete details).

parameter correlations explained by Metcalfe et al. (2000) are clearly visible, causing the good models to fall along lines in the plot rather than on a single point.

As expected, the optimal parameters from comparison of the observations to the complete grid of models were identical to those found using the genetic algorithm method. In fact, the identified periods led to lower rms residuals than any set of periods that included one of the possible aliases. Of the combinations with two periods replaced by their aliases, fits with lower residuals were achieved in three cases: (i) $f_1 \rightarrow f_1^-$ and $f_7 \rightarrow f_7^+$, (ii) $f_1 \rightarrow f_1^-$ and $f_7 \rightarrow f_7^-$ and (iii) $f_6 \rightarrow f_6^-$ and $f_7 \rightarrow f_7^-$. When either three or four periods were replaced with aliases, only one combination led to lower residuals: $f_1 \rightarrow f_1^-$, $f_5 \rightarrow f_5^+$ and $f_7 \rightarrow f_7^+$. Note that aliases of f_1 and f_7 appear in most of these alternative period lists, implying that they are relatively important to the outcome of the fit. Although lower residuals were possible using these various combinations of two or more alias periods, the optimal models in every such case are too massive and too cool to be reconciled with the spectral line fits for CBS 114 by Beauchamp et al. (1999).

5.2 Oxygen-core fit

The optimal set of model parameters found by the genetic algorithm for a pure O core extending to 0.95m/M$_*$ had a mass that was inconsistent with the measurements of Beauchamp et al. (1999) and a helium layer mass at the edge of our search range, near the theoretical limit before nuclear burning will occur at the base of the envelope. The second-best model had residuals only ~0.03 s higher and was similar to the optimal C-core model. The parameters of this model were

$$T_{\rm eff} = 25\,800\,{\rm K}$$

$$M_* = 0.640\,{\rm M}_\odot$$

$$\log(M_{\rm He}/M_*) = -3.96,$$

with rms period residuals $\sigma_P = 0.91$ s. The middle panel of Fig. 9 shows the calculated periods of this model along with the observations, plotted against the deviations from the mean period spacing. The fit is only slightly better than the C-core model, and is qualitatively similar.

The O-core models that were calculated by the genetic algorithm during the optimization process with rms period residuals smaller than 2.08 s are shown in the bottom half of Fig. 10. Although this is not a complete sampling of the parameter space, it is heavily sampled in regions where models produce better than average residuals. Again, the shade of each point indicates the relative quality of the match with black points within $\Delta\sigma_P = 0.03$ s of the optimal model, and the shades of grey at 3, 10, 25 and 40 times this difference. Note that because the optimal O-core model has residuals ~0.1 s lower than the optimal C-core model, the darkest grey points in the bottom half of Fig. 10 are actually better than the black points in the top half.

5.3 C/O-core fit

Since it may seem dubious to fit the seven observed periods of CBS 114 using a model with five free parameters, we proceed cautiously. To allow a systematic exploration of models with various internal C/O profiles, Metcalfe et al. (2001) used a simple parametrization that explored a general class of profiles similar to those used by Bradley et al. (1993). The parametrization fixes the oxygen mass fraction to its central value ($X_{\rm O}$) out to some fractional mass (q) where it then decreases linearly in mass to zero oxygen at $0.95m/M_*$.

Using this method, the optimal model parameters for the observed pulsation periods of CBS 114 were

$$T_{\rm eff} = 21\,000\,{\rm K}, \quad M_* = 0.730\,{\rm M}_\odot,$$

$$\log(M_{\rm He}/M_*) = -6.66, \quad X_{\rm O} = 0.61, \quad q = 0.51,$$

with rms period residuals $\sigma_P = 0.43$ s. All models within $\Delta\sigma = 0.03$ s of this fit had the same mass, temperature and helium layer mass at our sampling resolution of 0.005 M$_\odot$, 100 K and 0.05 dex, respectively. Only models with a central oxygen mass fraction within $\Delta X_{\rm O} = \pm 0.01$ and the optimal value of q had rms residuals within this range.

The calculated periods of this model are shown in the bottom panel of Fig. 9 along with the observed periods, plotted against the deviations from the mean period spacing. To evaluate whether or not this fit is better by an amount that justifies the addition of two free parameters, we can use the Bayes information criterion (BIC, following Koen & Laney 2000):

$${\rm BIC} = N_{\rm p}\left(\frac{\log N_{\rm obs}}{N_{\rm obs}}\right) + \log\sigma^2,$$

where $N_{\rm p}$ is the number of free parameters, $N_{\rm obs}$ is the number of observed periods and σ is the rms period residual of the optimal fit. The value of BIC must be lower for a decrease in σ to be considered significant. Our best three-parameter fit was the O-core model, which leads to a value of BIC = 0.28. This leads us to expect the residuals of a five-parameter fit to decrease to 0.69 s without being considered significant. The rms residuals of our five-parameter fit are substantially lower than 0.69 s, so the addition of the extra parameters seems to be justified, and the C/O fit is significantly better than the O-core model.

Even so, we might worry that our optimal model parameters may be less accurate than the values obtained for GD 358, owing to the smaller number of observed pulsation periods. To determine the magnitude of any systematic uncertainties owing to the smaller number of observed modes, we performed a new fit to the pulsation periods of GD 358, but using only the seven modes corresponding to those observed in CBS 114: $k = 8$, 9 and 11–15. When we compared the result of this fit with that using all 11 modes observed in GD 358, we found only small shifts to the optimal model parameters:

$$\Delta T_{\rm eff} = -500\,{\rm K}, \quad \Delta M_* = +0.015\,{\rm M}_\odot,$$
$$\Delta\log(M_{\rm He}/M_*) = -0.05, \quad \Delta X_{\rm O} = -0.02, \quad \Delta q = -0.01.$$

By analogy, we might expect our five-parameter fit to CBS 114 to represent a slight underestimate of the temperature and overestimate of the mass. Both potential biases help to explain part of the discrepancy between the mass and the temperature of our optimal model and the values inferred from the spectroscopic analysis of Beauchamp et al. (1999) ($T_{\rm eff} = 23\,300$; $\log g = 7.98$). Additional differences are expected since we have used different mixing-length parameters (ML3) from those of Beauchamp et al. (ML2/$\alpha = 1.25$). Metcalfe, Salaris & Winget (2002) quantified the offsets between fits to GD 358 using ML3 and ML2, and found them to be approximately the same size as the shifts owing to the smaller number of data points. Unfortunately, CBS 114 does not have a published parallax, so an independent constraint on the mass and temperature from the luminosity is not presently available.

6 CONCLUSIONS

We have presented time-resolved CCD photometry of the pulsating DB white dwarf stars CBS 114 and PG 1456+103. Our data, obtained with telescopes of only 0.75 and 0.9-m apertures, are sufficient for the extraction of useful asteroseismological information even for a star as faint as CBS 114 ($B \approx 17.2$). We have also shown that it is possible to understand the mode spectra of multiperiodic pulsating white dwarf stars from single-site observations in suitable cases (see Handler 2001 for another example). In other cases, such as PG 1456, this is not possible, and worldwide observing campaigns, e.g. with the Whole Earth Telescope, are necessary.

The frequency analysis of our measurements of CBS 114 resulted in the discovery of a mean period spacing of 37.1 ± 0.7 s in the independent modes of the star. Although no convincing evidence for rotational splitting within the modes was detected, we argued that the star pulsates in non-radial $\ell = 1$ g-modes.

We used our data set to check the sensitivity of the newly developed asteroseismological genetic algorithm methods (Metcalfe et al. 2000) to artefacts of data analysis, such as aliasing problems and our lack of assignments of the azimuthal order m to the observed modes. Encouragingly, our results are hardly affected by these shortcomings.

The most significant result from this work is based on the fact that the optimal mass and central oxygen mass fraction of CBS 114 can provide an independent measurement of the astrophysically important rate for the $^{12}C(\alpha, \gamma)^{16}O$ reaction, as was recently done for GD 358 (Metcalfe et al. 2002). In general, higher-mass white dwarfs are expected to have a lower central oxygen mass fraction, because the 3α rate rises faster with increasing density than the $^{12}C(\alpha, \gamma)^{16}O$ rate. Our optimal model for CBS 114 has a higher-mass and a lower central oxygen mass fraction than the optimal model for GD 358 (Metcalfe et al. 2001), thus being consistent with this general trend. A model of the internal chemical profile with the same mass as our fit to CBS 114 requires a rate for the $^{12}C(\alpha, \gamma)^{16}O$ reaction near $S_{300} = 180$ keV b to produce a central oxygen mass fraction of 0.61 (M. Salaris, private communication). This value is close to the rate derived from recent high-energy laboratory measurements ($S_{300} = 165 \pm 50$ keV b; Kunz et al. 2002). In contrast, the rate derived from the optimal model of GD 358 by Metcalfe et al. (2002) was significantly higher ($S_{300} = 370 \pm 40$ keV b). This suggests either that presently unknown sources of systematic uncertainty in our models must affect the analysis of GD 358 and CBS 114 in different ways, or that the two stars have different evolutionary origins, or both. An asteroseismological determination of the central oxygen mass fraction for additional DBV white dwarfs will help us to decide which of these scenarios is most likely.

ACKNOWLEDGMENTS

We thank Don Winget and Chuck Claver for permission to use their data of CBS 114, Maurizio Salaris for providing a new internal chemical profile to match our optimal model and Mike Montgomery for carefully reading a draft version of this paper.

REFERENCES

Beauchamp A., Wesemael F., Bergeron P., Liebert J., Saffer R.A., 1996, in Jeffery C.S., Heber U., eds, Hydrogen-Deficient Stars. ASP Conf. Ser. 96. Astron. Soc. Pac., San Francisco, p. 295
Beauchamp A., Wesemael F., Bergeron P., Fontaine G., Saffer R.A., Liebert J., Brassard P., 1999, ApJ, 516, 887
Bradley P.A., Winget D.E., 1994, ApJ, 430, 850
Bradley P.A., Winget D.E., Wood M.A., 1993, ApJ, 406, 661
Dziembowski W.A., 1977, Acta Astron, 27, 203
Grauer A.D., Bond H.E., Green R.F., Liebert J., 1988, AJ, 95, 879
Handler G., 2001, MNRAS, 323, L43
Handler G. et al., 1997, MNRAS, 286, 303
Kawaler S.D., 1987, in Cox A.N., Sparks W.M., Starrfield S.G., eds, Stellar Pulsations. Springer, Berlin, p. 367
Kjeldsen H., Frandsen S., 1992, PASP, 104, 413
Koen C., Laney D., 2000, MNRAS, 311, 636
Kunz R., Fey M., Jaeger M., Mayer A., Hammer J.W., Staudt G., Harissopulos S., Paradellis T., 2002, ApJ, 567, 643
Liebert J., 1986, Proc. IAU Coll. 87. D. Reidel Publishing Co., Dordrecht, p. 367
Metcalfe T.S., Nather R.E., Winget D.E., 2000, ApJ, 545, 974
Metcalfe T.S., Winget D.E., Charbonneau P., 2001, ApJ, 557, 1021
Metcalfe T.S., Salaris M., Winget D.E., 2002, ApJ, 573, 803
Montgomery M.H., O'Donoghue D., 1999, Delta Scuti Star Newslett., 13, 28, Univ. Vienna
Montgomery M.H., Metcalfe T.S., Winget D.E., 2001, ApJ, 548, L53
Nather R.E., Winget D.E., Clemens J.C., Hansen C.J., Hine B.P., 1990, ApJ, 361, 309
O'Donoghue D., 1995, Baltic Astron. 4, 519
Shipman H., 1997, in Isern J. et al., eds, White dwarfs: Proc. 10th European Workshop on White Dwarfs. Kluwer, Dordrecht, p.165
Sperl M., 1998, Master's thesis, Univ. Vienna
Tassoul M., 1980, ApJS, 43, 469
Vuille F. et al., 2000, MNRAS, 314, 689
Winget D.E., Claver C.F., 1988, IAU Circ. 4595
Winget D.E., Claver C.F., 1989, in Wegner G., ed., White dwarfs. Proc. IAU Colloq. 114, Springer, Berlin, p. 290
Winget D.E. et al., 1994, ApJ, 430, 839
Wolff B., Koester D., Montgomery M.H., Winget D.E., 2002, A&A, 388, 320

This paper has been typeset from a TEX/LATEX file prepared by the author.